

RSC Advances



This is an *Accepted Manuscript*, which has been through the Royal Society of Chemistry peer review process and has been accepted for publication.

Accepted Manuscripts are published online shortly after acceptance, before technical editing, formatting and proof reading. Using this free service, authors can make their results available to the community, in citable form, before we publish the edited article. This *Accepted Manuscript* will be replaced by the edited, formatted and paginated article as soon as this is available.

You can find more information about *Accepted Manuscripts* in the [Information for Authors](#).

Please note that technical editing may introduce minor changes to the text and/or graphics, which may alter content. The journal's standard [Terms & Conditions](#) and the [Ethical guidelines](#) still apply. In no event shall the Royal Society of Chemistry be held responsible for any errors or omissions in this *Accepted Manuscript* or any consequences arising from the use of any information it contains.

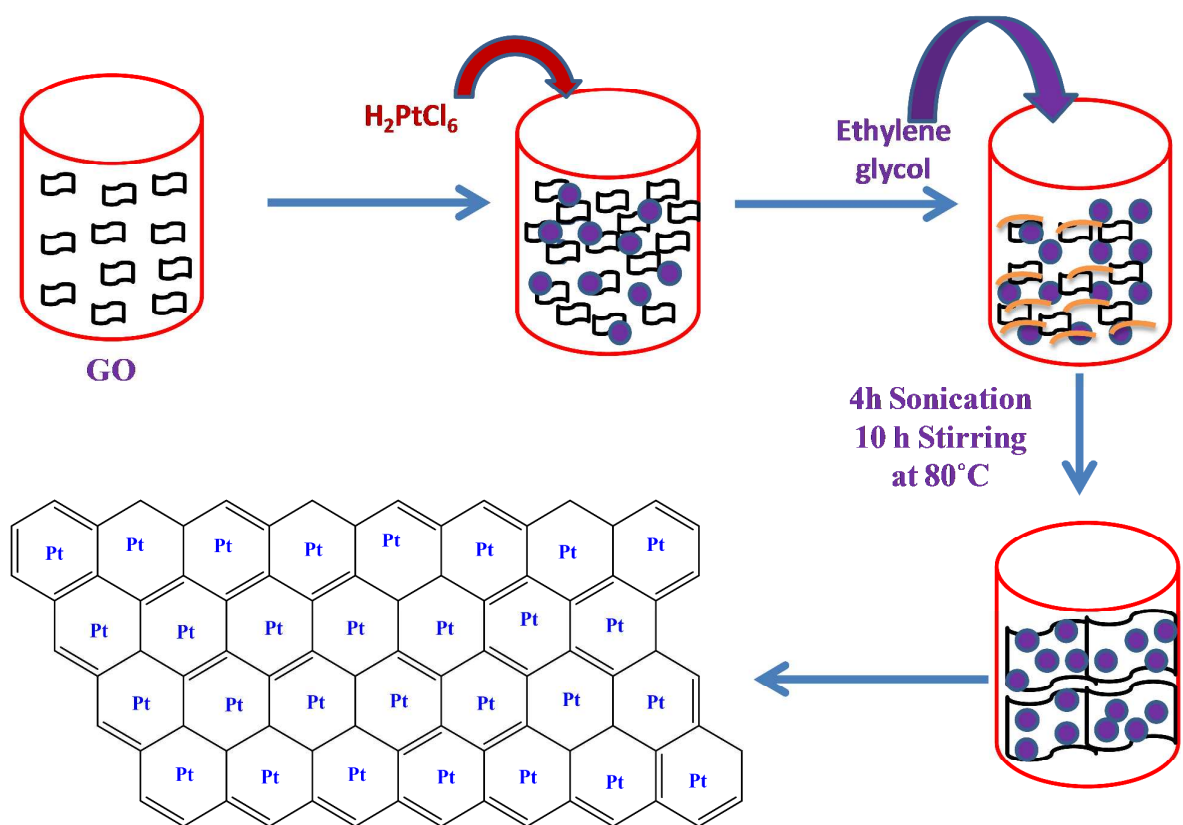


Fig. 1: Schematic representation of the complete synthesis of Pt / RG process.

Platinum supported reduced graphene catalyst to enhance the hydrogenation of nitro compound activity

Madhan Mohan Raju and Deepak K. Pattanayak[†]

CSIR - Central Electrochemical Research Institute, Karaikudi - 630006, TamilNadu, India

Abstract:

We have investigated a simple approach for preparation of platinum (Pt) decorated graphene and N- doped Pt decorated graphene nano sheets in presence ethylene glycol (EG) for catalytic hydrogenation of nitro compounds. The presence of EG not only triggers the mono dispersion of Pt nano particles (NPs) of 2 to 6 nm particle size and also its homogeneous distribution on graphene nano sheets without any agglomeration. Results showed that these Pt-nano particles supported graphene as well as Pt, N- doped graphene nano sheets enhanced the catalytic reduction of 4-nitro aniline (4-NA) to para- phenyl di aniline (p-PDA) in the presence aqueous solution of NaBH₄. This two dimensional Pt supported reduced graphene sheet with large surface area showed enhanced catalytic properties compared to other noble metal nano particles.

Keywords: Pt reduced graphene; 4-nitro aniline; catalysis; FE-SEM.

[†]Corresponding author: Deepak K. Pattanayak, E-mail: pattanayak1977@gmail.com;
Tel No: +91-4565-241397

1. Introduction

Single atom thick, mono layer sheets with sp^2 carbon atoms arranged in a honeycomb lattice of graphene was successfully prepared in 2004.¹⁻⁴ Since then, it has attracted tremendous research interest owing to its intriguing electronic,⁵ optical,⁶⁻⁸ physical, chemical and mechanical properties.⁹⁻¹² This graphene is derived from graphene oxide (GO) by several methods that include micromechanical exfoliation, thermal expansion of graphite,¹³⁻¹⁵ and simple chemical reduction of exfoliated GO.¹⁶⁻¹⁹ Among these methods, chemical reduction of exfoliated GO is the most suitable approach for low cost and large scale production of graphene nanosheets.¹⁸ GO has large surface area, and, readily disperse in organic solvents such as dimethylformamide (DMF), N-methyl-2-pyrrolidone (NMP) etc. to yield stable dispersion by simple sonication on account of the presence of oxygen containing functional groups on its surfaces and edges.²⁰ Furthermore, these oxygen functional groups act as anchoring sites for the binding of various metal nanoparticles to develop metal decorated graphene nanosheets and used as catalyst for various chemical reactions.²¹ One of these processes exploits the ability of non-noble metals such as Al,^{22, 23} Fe,²⁴ Zn,²⁵⁻²⁸ Ni²⁹ and Mg³⁰ to act as reducing agents. These nano particles can readily attract oxygen functional groups and bond with hydrogen in acidic medium from the GO sheets. The other process is based on the use of noble metals such as Pd,³¹ Pt,^{32, 33} and Au³⁴ nano particles of improved stability and dispersion on reduced graphene (RG). At the same time, these nano particles improve the catalytic properties of RG nano sheets.

Platinum (Pt) nano particles due to their unique chemical and physical properties are widely used in the process of catalysis for the reduction of 4-nitro aniline (4-NA),³⁵ and oxidation of benzyl alcohols^{36, 37} and propylene epoxidation etc.^{38, 39} Further, Pt / RuO₂ and Pt / TiO₂ catalysts show high activities in the electro-oxidation of primary alcohols.^{40, 41} The catalytic

activities of these catalysts are widely related to the selection of oxide support and oxide substrates.⁴² Although, noble metal such as Pt, Au, Pd etc. are commonly used as catalyst for various oxidation and reduction reactions, high cost and less abundance is a serious concern among the researchers. This necessitates developing either non noble metal based catalyst or minimum consumption of noble metal while maintaining the same catalytic activities.

In the present study, we investigated a very simple chemical reduction method to homogeneously decorate Pt nano particles with extremely small size on RG sheets (Pt/RG) and N- doped RG sheets (Pt/RG-N). Subsequently, the catalytic performance of Pt/RG and Pt/RG-N was evaluated using nitro compound as an example.

2. Experimental section

2.1 Chemicals

Graphite powder, sulphuric acid, ethylene glycol, phosphoric acid are purchased from Sigma Aldrich, Switzerland and these chemicals are used for preparation of graphene oxide (GO). Potassium permanganate is supplied by sd fine-chem. Ltd., India. Hexa chloro platinumic acid (H_2PtCl_6) used as Pt source is purchased from Sigma Aldrich.

2.2 Synthesis of graphene oxide

Graphene oxide (GO) has been synthesized following the improved method reported by Tour et al where graphite powder was used as the starting material.^{43, 44} In this method, 2 g of graphite powder was thoroughly mixed with sulphuric acid and phosphoric acid (9:1 ratio) (Alfa aesar) mixture at room temperature by magnetic stirring. Potassium permanganate crystals (14 g) were then slowly added to this mixture. The resultant mixture was stirred well by keeping the temperature at 90 °C for 24 h. Subsequently, 14 mL of 30 % H_2O_2 (Alfa aesar) was added to this mixture, after keeping the mixture in an ice bath, the solution was then vacuum filtered and

washed with deionized (DI) water, 5 % HCl and ethanol for 3 cycles. The resultant filtrate (GO) is soaked in ether and dried in a vacuum oven at 80 °C for 24 h.

2.3 Synthesis of Pt decorated reduced graphene (Pt/RG)

Pt nano particles were decorated on GO sheets by chemical reduction of hexachloroplatinic acid (H_2PtCl_6) in ethylene glycol (EG) solution. In a typical procedure, 1 mL aqueous solution of 0.04 M H_2PtCl_6 and 10 mL of DI water and 50 mg of GO powder were added into 40 mL EG in a 250 mL beaker. The mixture was first ultrasonically treated for 4 h to ensure the GO to be uniformly dispersed in EG - water solution. The reduction reaction was performed at 80 °C with continuous stirring up to 10 h. The colloidal mixture was collected from the beaker, washed with water using vacuum filtrate (Axiva set up) and cellulose nitrate filter paper (0.8 μm) in order to make the $\text{pH} \sim 7$. The final product was collected from vacuum filter and dried at 90 °C for 12 h in an oven. Fig. 1 shows the schematic representation of the complete synthesis process. For comparison similar condition of Pt loaded Vulcan carbon (home made Pt/C) was synthesized.

2.4 Synthesis of N- doped Pt decorated reduced graphene (Pt/RG-N)

The GO (0.1 g) was dispersed in DI water (93 mL) and 7 mL of hydrazine hydrate added to this GO solution with continuous stirring up to 2 h. After that, 3 mL of ammonium hydroxide was added to this solution and kept in a Teflon autoclave. The autoclave was kept in an oven at 180 °C for 12 h. The residue was collected and dispersed in water and vacuum filtrated using cellulose nitrate filter paper. This residue was washed several times with DI water to make the $\text{pH} \sim 7$ and allowed to dry at 50 °C for 24 h in an oven. The resultant powder was collected and is known as N- doped graphene.⁴⁴ Synthesis of Pt/RG-N from N- doped graphene (50 mg) was carried out by adding 40 mL of EG, 10 mL DI water and 1 mL of 0.04 M H_2PtCl_6 and ultra

sonicated for 4 h. In order to make uniform dispersion, the solution was stirred while maintaining the temperature at 80°C for 10 h. The colloidal mixture was then collected, washed with water using vacuum filtrate using cellulose nitrate filter paper (0.8 µm) in order to make the $P^H \sim 7$. The final product Pt/RG-N was collected from vacuum filtrate and dried at 90°C for 12 h in an oven. Subsequently, this Pt/RG-N catalyst powder was characterized by various characterization tools.

2.5 Characterization

The structure, morphology and texture of Pt/RG and Pt/RG-N catalyst were characterized by powder X-ray diffraction (XRD), field emission scanning electron microscopy (FE-SEM) and transmission electron microscopy (TEM) and high resolution TEM (HR-TEM). In order to confirm the crystal structure and phase purity of the samples, powder X-ray diffraction patterns were recorded on a Bruker D 8 Advance X-ray diffractometer with Cu K α ($\lambda = 1.5405 \text{ \AA}$) radiation in the range of 10-70° (2 θ). The morphology and structural properties of the as-synthesized Pt/RG and Pt/RG-N were observed using a FE-SEM (Carl Zeiss SUPRA 55VPFEI, Germany). TEM and HR-TEM images of samples were taken using a FEI TECNAI G² 20 and FEI TECNAI TF 20 the Netherland with an accelerating voltage of 200 kV, respectively. TEM samples were prepared (mixing DMF and sample under sonication for 45 min) by placing a drop of solution on a carbon coated copper grid and drying under UV light selected area electron diffraction (SAED) pattern were taken for Pt/RG and Pt/RG-N catalyst samples. Particle size of Pt nano particles on graphene sheets were calculated from TEM images using image J software. Raman measurements were carried out using Renishaw (UK) In Via Raman microscope with 632.8 nm wavelength incident laser light and spectra were collected using a back scattering geometry of materials within an acquisition time of 40 seconds The crystallite size can be

determined according to the Tuinstra-Koenig (TK) relation $L_a \text{ (nm)} = (2.4 \times 10^{-10}) \lambda (I_D / I_G)^{-1}$ Where λ = Raman excitation wavelength 632.8 nm.⁴⁵ Presence of functional groups and their stretching and bending vibrations in GO, Pt/RG as well as Pt/RG-N were observed using FTIR (BRUKER OPTIK GMBH, Germany; Model no TENSOR 27). A Shimadzu balance of model 220D with 10 mg sensitivity was used for weighing the materials. UV- visible (UV-Vis) absorption spectra were recorded with a Unico (model 4802) UV-Vis-NIR spectrophotometer equipped with a 1 cm quartz cuvette holder for liquid samples.

2.6 Catalytic reduction of aromatic nitro compounds

The catalytic reduction of aromatic nitro compounds was studied using Pt/RG, Pt/RG-N and Pt/C as catalyst. The catalysis study was carried out using 4- nitro aniline (4-NA) as a model example. In this process, 0.5 mL of (10^{-3} M) 4-NA mixed in 4 mL of DI water and stirred for 5 min to obtain a homogeneous solution. Subsequently, 1 mL of different concentration (10, 20, 25 mM) of NaBH_4 solution was added into the mixture and shaken well. Finally 0.5 mL of different amount of catalyst (12.5, 25 and 37.5 μg) of Pt/RG and Pt/RG-N solution was added to the reaction mixture and UV- Vis spectra were recorded continuously over different time intervals until complete reduction of aromatic nitro compound. The completion of reaction was confirmed by the color change from light yellowish 4-NA solution to a colorless *para* – phenyldiamide (*p* - PDA) as well as from the absorption bands in the UV-Vis spectrum. In another set up experiment, amount of catalyst was varied while keeping NaBH_4 concentration same (25 mM) and the similar experiment was carried out to observe the effect of catalyst amount on reduction process.

3. Results and discussions

Fig. 2 shows the XRD pattern of graphite, GO, RGO, Pt/RG and Pt/RG-N catalyst. It can be seen from Fig. 2 that as-purchased graphite powder has a sharp diffraction peak observed at a 2θ of 26.54° (JCPDS # 656212) with interlayer spacing (d value) of 0.33 nm.⁴⁴ On subsequent oxidation of graphite powder, the same plane was shifted to 11.07° in the case of GO while increasing the d value from 0.33 nm to 0.79 nm. It is well known that GO shows a sharp diffraction peak at $2\theta = 11.2^\circ$ and the same results were observed in the present study.⁴⁴ This suggests the complete exfoliation of graphite powder during the chemical synthesis route and the presence of sharp plane (002) confirmed the formation of few layer of GO sheets. RGO showed a broad peak at 23.87° with interlayer spacing of 0.37 nm, which is half of the value of GO (0.79 nm) due to the removal of intercalated oxygen containing functional groups. However, in the case of Pt/RG sample the same plane (002) was shifted from 11.2° to 24.4° along with other additional sharp diffraction peaks at 39.6° , 46.2° , 67.5° and 81.4° that corresponds to the (111), (200), (220) and (311) planes of Pt, respectively. This indicates the formation of face centered cubic (FCC) Pt (JCPDS # 040802) by the complete reduction process of H_2PtCl_6 in the presence of EG solution. Presence of (002) plane in the XRD spectrum indicates the hexagonal structure of the graphene sheet and the nature of the graphene sheet was not affected by the decoration of Pt nano particles on its surface. The XRD pattern of Pt/RG-N was similar to that of Pt/RG, although interlayer spacing was little higher than that of Pt/RG possibly due to the presence of N- doping in the graphene sheet. Confirmation of the presence of N- in the graphene sheet will be discussed in the latter section.

Raman spectroscopy is a useful technique to analyze the formation of defect in the graphene layers during the reduction of GO as well as doping of nitrogen into graphene lattice.

Fig. 3 shows the Raman spectra of graphite, GO, Pt/RG and Pt/RG-N catalyst. From Fig. 3, it can be seen that the defects were created between the edges of graphite during the oxidation process to obtain GO. Two prominent peaks corresponding to the well documented D and G bands were observed at 1320-1350 cm^{-1} and 1570-1600 cm^{-1} , respectively. The G band is assigned to the E_{2g} of C sp^2 atoms, while the D band corresponds to the first order scattering of all A_1 symmetry disordered carbon materials.^{46, 47} Both the peaks appeared in all cases although the intensity was different that corresponds to the amount of defects created in the graphene sheet. The intensity ratio of the D and G band (I_D / I_G) were 0.95, 1.08 and 1.13, and the crystallite size 36.48, 39.55 and 43.39 nm for GO, Pt/RG and Pt/RG-N, respectively as shown in Table 1. The increase in I_D / I_G ratios for Pt/RG and Pt/RG-N catalyst as compared to GO is reasonable because of chemical reduction of GO. This indicates that the conjugated graphene network (sp^2 carbon) is re-established and the graphene network became thinner than the original graphite layer leading to an increase in I_D / I_G ratio.⁴⁸ This indicates that GO in Pt/RG and Pt/RG-N catalyst has been well deoxygenated and reduced.

FTIR spectroscopy is used to understand the presence of different functional groups in terms of their stretching and bending vibrations. Fig. 4 shows the FTIR spectra of GO, Pt/RG and Pt/RG-N catalyst. As-synthesized GO was intercalated with different oxygen functionalities which are covalently bonded to the hexagonal plane of carbon such as epoxies (C-O-C), carboxyl (-COOH), carbonyl (C=O), alkenes (C=C) and hydroxyl (-OH) groups. The functional groups such as sp^2 hybridized C=C peak at 1580-1600 cm^{-1} , carbonyl at 1720 cm^{-1} , hydroxyl stretching at 3200 -3600 cm^{-1} and epoxy group (C-O-C) stretching at 1248 cm^{-1} were observed.⁴⁴ This result indicates edge defects of GO due to the presence of hydroxyl, carbonyl and epoxy groups etc. In the case of Pt/RG, epoxy (C-O-C), carbonyl (C=O) and alkene (C=C) groups were

observed while other functional groups were reduced in presence of EG. Functional groups such as C-N, alkene (C=C) and N-H stretching vibration peaks were observed at 1180-1262 cm^{-1} , 1580-1600 cm^{-1} and 3400 cm^{-1} , respectively for Pt/RG-N catalyst.⁴⁴

The morphology of the Pt/RG and Pt/RG-N catalyst was observed by FE-SEM, TEM and HR-TEM, and the results are shown in Fig. 5. It can be seen from FE-SEM image that Pt/RG-N catalyst prepared from the reduction of few layers of GO sheets completely exfoliated to two dimensional sheets, and, Pt nano particles were uniformly decorated on the RG surface (Fig. 5a). Corresponding EDS spectra (Fig. 5b) confirmed the presence of Pt and nitrogen in Pt/RG-N sheet. Figure 5c & d shows the TEM images of Pt/RG and Pt/RG-N catalyst and their corresponding SAED pattern as inset. Pt nano particles of particle size 2 to 6 nm (shown in inset) were uniformly dispersed on the graphene sheets without any aggregation. In Pt/RG and Pt/RG-N samples, small size Pt nano particles were observed, and, EG were found to be a good reducing agent as well as a suitable solvent for dispersion of Pt nano particles uniformly in the graphene sheet without creating any agglomeration. SAED pattern confirms the hexagonal graphene sheet as shown in the inset of Fig. 5c & d. The particle size of Pt in Pt/RG as well as Pt/RG-N catalysts was found to be almost same and uniformly distributed over the graphene surface. The high resolution TEM image of Pt/RG-N in Fig. 5e clearly demonstrates the oriented and ordered lattice fringes of Pt nano particles. The d-spacing value of 0.212 nm corresponds to Pt (111) as seen in Fig. 5e inset.

X- ray photo electron spectroscopy (XPS) studies were carried out to further confirm the presence of nitrogen, Pt and their bonding configurations in Pt/RG and Pt/RG-N catalyst and the result is shown in Fig. 6a&b. XPS spectra of Pt4f in Pt/RG and Pt/RG-N catalyst confirmed the

presence of Pt on the surface of graphene sheet and are shown in Fig. 6a. The binding energy of Pt in Pt/RG and Pt/RG-N are 71.12 (Pt 4f_{7/2}) 74.64 (Pt 4f_{5/2}) and 71.54 (Pt 4f_{7/2}) 74.94 (Pt 4f_{5/2}), respectively. This indicates that Pt peak was shifted towards higher binding energy in the case of Pt/RG-N catalyst compared to Pt/RG because of Pt bonded to nitrogen. Deconvolution of the Pt4f region shows the presence of two pairs of doublets (Pt/RG sample is shown in inset of Fig. 6a). The most intense doublet with binding energy of 71.3 (Pt 4f_{7/2}) and 74.5 eV (Pt 4f_{5/2}) is attributed to the metallic Pt and peaks at 72.2 (Pt 4f_{7/2}) and 75.6 eV (Pt 4f_{5/2}) could be assigned to Pt that anchored with the C-O group in RG. In both Pt/RG as well as Pt/RG-N catalyst, from the area under the curve, we can find amount of Pt in metallic state is higher compared to Pt-O-C bonded. Metallic Pt is expected to anchor during the reduction of nitro compound compared to Pt-O-C bonded Pt in the catalyst.⁴⁵ Similarly, the bonding configurations of nitrogen in Pt/RG-N was characterized by high-resolution N1s spectra (Fig. 6b). The deconvolution of N1s spectra of Pt/RG-N shows four peaks at 398.2, 399.5, 401.1 and 402.6 eV. The peaks with lower binding energy located at 398.2 and 399.5 eV corresponds to pyridinic like N-C bonding and pyrrolic like N-C bonding, respectively.⁴⁴ When carbon atoms within the graphene layers are substituted by nitrogen atoms in the form of graphitic nitrogen, the corresponding peak in the high-resolution N1s spectra is observed at 401.1 eV. Peak at 402.6 eV is attributed to the oxidized nitrogen. A typical complete survey spectrum of Pt/RG-N shows the presence of O1s, N1s, C1s and Pt4f elements (supporting information Fig. S-1).

The reduction of 4-NA to p-PDA in presence of NaBH₄ was used as a model reaction to characterize the catalytic performance of Pt/RG and the result is shown in Fig. 7. It can be seen from Fig 7a-c that the intensity of 4-NA peak at 380 nm was gradually decreased with respect to time while two new adsorption peaks at 239 and 304 nm appeared due to the formation of p-

PDA.^{49, 50} The intense adsorption peak of 4-NA (380 nm) took 8, 5 and 4 min to reduce to p-PDA when the Pt/RG catalyst loading was increased in the order of 12.5, 25 and 37.5 μg , respectively. This indicates that the increase in Pt/RG catalyst loading decrease the time period of reduction process. In the time dependent catalysis reaction, the rate of reaction was calculated from $\ln(\text{con})$ vs time (min) in different time frames and is shown in Fig. 7a1-c1. The results indicate that reduction process follows a pseudo first order reaction. In case of 12.5 μg of Pt/RG catalyst and 25 mM NaBH_4 concentration the reduction process took 8 min with rate constant value $54 \times 10^{-2} \text{ min}^{-1}$ with correlation coefficient and standard deviation values 0.9961 and 0.0127, respectively (Fig. 7a₁). When Pt/RG catalyst loading was increased from 12.5 to 25 μg , the time taken for the reduction process was decreased from 8 to 5 min, respectively with rate constant value $56 \times 10^{-2} \text{ min}^{-1}$ with correlation coefficient and standard deviation values 0.954 and 0.0617, respectively (Fig. 7b₁). Further increase in Pt/RG catalyst loading to 37.5 μg , it took 4 min to completely reduce the 4-NA with a rate constant value $63 \times 10^{-2} \text{ min}^{-1}$ with correlation coefficient and standard deviation values 0.942 and 0.0735, respectively (Fig. 7c₁). This faster reduction is ascribed to the Pt metal loading i.e. 1.37 μg , 2.74 μg and 4.12 μg in the Pt/RG catalyst of 12.5 μg , 25 μg and 37.5 μg , respectively. Table 2 summarizes various types of nanocatalysts used in the literature to that of Pt/RG catalyst in the present study. Performance of Pt/RG catalyst is found to be better in comparison to the reported literatures. Reduction of 4-NA to p-PDA using only NaBH_4 and different concentrations of NaBH_4 in presence of catalyst is discussed in supporting information Fig. S-2 and Fig S-3.

Based on the results obtained in the present study, the complete reduction process of yellow color 4-NA solution to colorless p-PDA and the general mechanism of reduction of nitro compound are shown in Fig. 8. The catalytic decomposition of NaBH_4 in presence of Pt/RG

catalyst begins with release of electrons from catalyst producing H-Pt and PtBH_3^- as reactive intermediates⁵¹. These species are believed to be responsible for the reduction of p-NA to p-PDA. In general, precious metal nanoparticles have high activity, excellent efficiency, and hence act as active catalysts for many electron-transfer reactions. The catalytic properties of precious metal nanoparticle depend on the size and distribution of the nanoparticles and on the interactions between the metal nanoparticles and the nature of the support. The excellent performance of the Pt catalyst supported graphene is possibly due to the morphology, particle size and distribution. In the present study, ethylene glycol effectively disperses these fine Pt nanoparticles on graphene support and thus developed catalyst is found to be effective for reduction of nitro compounds.

We made an attempt to compare the catalytic activity of Pt/RG, Pt/RG-N and home made Pt/C (same catalyst loading) expecting the enhancement of catalytic activity in presence of N-doping into the graphene sheets. However, we could not observe any remarkable enhancement in the catalytic activity of Pt/RG-N catalyst. The catalytic activity of N-doped graphene in similar concentration of NaBH_4 showed about 20% reduction of 4 NA after 2hrs (supporting information Fig. S-4). The catalytic activity of N-doped graphene might be improved by increasing the concentration of NaBH_4 solution. From the present study, Pt in Pt/RG-N catalyst is found to be dominating the reduction process compared to nitrogen in the N-doped graphene. Further studies are in progress to understand the catalytic activity of Pt/RG-N with respect to the amount of nitrogen doping into the graphene nano sheet and will be reported later. This may lead to the development of Pt/RG-N catalyst with minimum consumption of noble metal such as Pt. Similarly, studies on home made Pt /C catalyst showed lower catalytic activity compared to Pt/RG and Pt/RG-N catalyst as shown in Fig. S-5. The lower catalytic activity of Pt/C might be

due to lower conductivity of Vulcan carbon compared to graphene. The reduced product of 4-NA to *p*-PDA is widely used for industrial purposes for making azo dyes and antioxidants and is well known as an important intermediate for the manufacture of antipyretic drugs.⁵² The catalyst support prepared from Pt decorated RG was found to be suitable for continuous reduction of aromatic nitro compounds as seen in the present study.

4. Conclusion

In conclusion, we have synthesized Pt/RG and Pt/RG-N through a simple chemical reduction using EG as a reducing agent. EG not only reduced the GO to RG and also helped the Pt nano particles of size 2 to 6 nm uniformly distributed on graphene sheets without any agglomeration. The Pt/RG have also been tested for a catalytic reaction. The catalytic reduction of organic nitro compounds and the catalytic rate was found to be faster for Pt/RG catalyst compared to other Au, Ag and Cu NPs. The uniform size distribution of Pt NPs, high dispersion ability on graphene and the effective electron transfer makes the Pt/RG an efficient catalyst in the reduction of aromatic nitro compounds.

Acknowledgements:

The authors acknowledge Dr. T. N. Narayanan, M. Praveen Kumar and Dr. R. Senthil Kumar for their useful discussion during the experiment. Mr. A. Rathish Kumar for TEM, Mr. J. Kennedy for XPS analysis and financial support from MULTIFUN (CSC0101) is highly acknowledged. Dr. S. Kundu useful discussion on UV Vis measurement is also appreciated.

References:

1. M. I Katsnelson, K. S. Novoselov and A. K Geim, *Nat. Phys.* 2006, **2**, 620–625.
2. K. S. Novoselov, Z. Jiang, Y. Zhang, S. V. Morozov, H. L. Stormer, U. Z. eitler, J. C. Maan, G. S. Boebinger, P. Kim and A. K. Geim, *Science* 2007, **315**, 1379.

3. F. Wang, Y. Zhang, C. Tian, C. Girit, A. Zettl, M. Crommie and Y. R. Shen, *Science* 2008, **320**, 206–209.
4. K. S. Novoselov, A. K. Geim, S. V. Morozov, D. Jiang, M. I. Katsnelson, I. V. Grigorieva, S. V. Dubonos and A. A. Firsov, *Nature*, 2005, **438**, 197–200.
5. Y. Zhang, J. W. Tan, H. L. Stormer and P. Kim, *Nature*, 2005, **438**, 201–204.
6. P. Blake, P. D. Brimicombe, R. R. Nair, T. J. Booth, D. Jiang, F. Schedin, L. A. Ponomarenko, S. V. Morozov, H. F. Gleeson and E. W. Hill, *Nano Lett.* 2008, **8**, 1704–1708.
7. A. R. Wright, X. G. Xu, J. C. Cao and C. Zhang, *Appl. Phys. Lett.* 2009, **95**, 072101-1-072101-3.
8. X. Xu, N. M. Gabor, J. S. Alden, A. M. vander Zande and P. L. McEuen, *Nano Lett.* 2010, **10**, 562–566.
9. C. Lee, X. D. Wei, J. W. Kysar and J. Hone, *Science*, 2008, **321**, 385–388.
10. S. Stankovich, R. D. Piner, S. T. Nguyen and R. S. Ruoff, *Carbon*, 2006, **44**, 3342–3347.
11. J. Pyun, *Angew. Chem., Int. Ed.*, 2011, **50**, 46.
12. T. Wu, X. R. Wang, H. X. Qiu, J. P. Gao, W. Wang and Y. Liu, *J. Mater. Chem.*, 2012, **22**, 4772–4779.
13. K. S. Novoselov, A. K. Geim, S. V. Morozov, D. Jiang, Y. Zhang, S. V. Dubonos, I. V. Grigorieva and A. A. Firsov, *Science*, 2004, **306**, 666–669.
14. K. S. Kim, Y. Zhao, H. Jang, S. Y. Lee, J. M. Kim, K. S. Kim, J. H. Ahn, P. Kim, J. Y. Choi and B. H. Hong, *Nature*, 2009, **457**, 706–710.
15. H. C. Schniepp, J. L. Li, M. J. McAllister, H. Sai, M. Herrera-Alonso, D. H. Adamson, R. K. Prud'homme, R. Car, D. A. Saville and I. A. Aksay, *J. Phys. Chem. B*, 2006, **110**, 8535–8539.

16. S. Stankovich, D. A. Dikin, R. D. Piner, K. A. Kohlhaas, A. Kleinhammes, Y. Jia, Y. Wu, S. T. Nguyen and R. S. Ruoff, *Carbon*, 2007, **45**, 1558–1565.
17. X. B. Fan, W. C. Peng, Y. Li, X. Y. Li, S. L. Wang, G. L. Zhang and F. B. Zhang, *Adv. Mater.*, 2008, **20**, 4490–4493.
18. D. Li, M. B. Muller, S. Gilje, R. B. Kaner and G. G. Wallace, *Nat. Nanotechnol.*, 2008, **3**, 101–105.
19. H. J. Shin, K. K. Kim, A. Benayad, S. M. Yoon, H. K. Park, I. S. Jung, M. H. Jin, H. K. Jeong, J. M. Kim, J. Y. Choi and Y. H. Lee, *Adv. Funct. Mater.*, 2009, **19**, 1987–1992.
20. A. Buchsteiner, A. Lerf and J. Pieper, *J. Phys. Chem. B*, 2006, **110**, 223–228.
21. K. Jasuja and V. Berry, *ACS Nano*, 2009, **3**, 2358–2366.
22. Z. Fan, K. Wang, T. Wei, J. Yan, L. Song and B. Shao, *Carbon*, 2010, **48**, 1686–1689.
23. V. H. Pham, H. D. Pham, T. T. Dang, S. H. Hur, E. J. Kim, B. S. Kong, S. Kim and J. S. Chung, *J. Mater. Chem.*, 2012, **22**, 10530–10536.
24. Z. J. Fan, W. Kai, J. Yan, T. Wei, L.-J. Zhi, J. Feng, Y. Ren, L. P. Song and F. Wei, *ACS Nano*, 2011, **5**, 191–198.
25. X. Mei and J. Ouyang, *Carbon*, 2011, **49**, 5389–5397.
26. Y. Liu, Y. Li, M. Zhong, Y. Yang, Y. Wen and M. Wang, *J. Mater. Chem.*, 2011, **21**, 15449–15455.
27. R. S. Dey, S. Hajra, R. K. Sahu, C. R. Raj and M. K. Panigrahi, *Chem. Commun.*, 2012, **48**, 1787–1789.
28. S. Yang, W. Yue, D. Huang, C. Chen, H. Lin and X. Yang, *RSC Adv.*, 2012, **2**, 8827–8832.
29. P. Liu, Y. Huang and L. Wang, *Mater. Lett.*, 2013, **91**, 125–128.

30. R. Krishna, E. Titus, L. C. Costa, J. C. J. M. D. S. Menezes, M. R. P. Correia, S. Pinto, J. Ventura, J. P. Araujo, J. A. S. Cavaleiro and J. J. A. Gracio, *J. Mater. Chem.*, 2012, **22**, 10457–10459.
31. B. K. Barman, P. Mahanandia and K. K. Nanda, *RSC Adv.*, 2013, **3**, 12621–12624.
32. M. Liang, J. Wang, B. Luo, T. Qiu and L. Zhi, *Small*, 2012, **8**, 1180–1184.
33. T. T. Dang, V. H. Pham, B. K. Vu, S. H. Hur, E. W. Shin, E. J. Kim and J. S. Chung, *Mater. Lett.*, 2012, **86**, 161–164.
34. V. H. Pham, T. T. Dang, K. Singh, S. H. Hur, E. W. Shin, J. S. Kim, M. A. Lee, S. H. Baeck and J. S. Chung, *J. Mater. Chem. A*, 2013, **1**, 1070–1077.
35. K. Jasuja, J. Linn, S. Melton and V. Berry, *J. Phys. Chem. Lett.*, 2010, **1** (12) 1853–1860.
36. A. Abad, P. Concepcin, A. Corma and H. Garca, *Angew. Chem., Int. Ed.*, 2005, **44**, 4066.
37. A. Abad, C. Almela, A. Corma and H. Garcia, *Chem. Commun.*, 2006, 3178–1380.
38. M. Haruta, *Chem. Rec.*, 2003, **3**, 75–87.
39. A. S. K. Hashimi and G. J. Hutchings, *Angew. Chem., Int. Ed.*, 2006, **45**, 7896–7936.
40. X. P. Qiu, L. Cao, F. Scheiba, C. Roth, F. Schweiger, C. Cremers, U. Stimming, H. Fuess, L. Q. Chen and W. T. Zhu, *Angew. Chem., Int. Ed.*, 2006, **45**, 5315-5319.
41. S. J. Yoo, T. Y. Jeon, K. S. Lee, K. W. Park and Y. E. Sung, *Chem. Commun.*, 2010, **46**, 794-796.
42. P. J. Miedziak, Z. R. Tang, T. E. Davies, D. I. Enache, J. K. Bartley, A. F. Carley, A. A. Herzing, C. J. Kiely, S. H. Taylor and G. J. Hutchings, *J. Mater. Chem.*, 2009, **19**, 8619-8627.
43. D. C. Marcano, D. V. Kosynkin, J. M. Berlin, A. Sinitskii, Z. Sun, A. Slesarev, L. B. Alemany, W. Lu and J. M. Tour, *ACS Nano*, 2010, **4**(8), 4806-4814.
44. M. Praveen Kumar, T. Kesavan, G. Kalita, P. Ragupathy, T. N. Narayanana and D.

- K. Pattanayak, *RSC Adv.*, 2014, **4**, 38689-38697.
45. R. Niewa, J. Wang, L. Wang, Y. Qian, P. Chen and Z. Hou, *Carbon*, 2011, **50**, 586-596.
46. F. Tuinstra and J. L. Koenig, *J. Chem. Phys.*, 1970, **53**, 1126.
47. D. Graf, F. Molitor, K. Ensslin, C. Stampfer, A. Jungen, C. Hierold and L. Wirtz, *Nano Lett.*, 2007, **7**, 238-242.
48. C. Xu, X. Wang and J. W. Zhu, *J. Phys. Chem. C*, 2008, **112**, 19841-45.
49. S. K. Ghosh, M. Mandal, S. Kundu, S. Nath and T. Pal, *Applied Catalysis A*, 2004, **268**, 61-66.
50. J. Feng, L. Su, Y. Ma, C. Ren, Q. Guo and X. Chen, *J. Chem. Engg.*, 2013, **221**, 16-24.
51. S. Pandey, S B. Mishra. *Carbohydrate Polymers*, 2014, **113**, 525-531
52. Y. Du, H. Chen, R. Chen and N. Xu, *Appl. Catal. A*, 2004, **277**, 259-264.
53. U. Nithiyantham, S. Rao Ede and S. Kundu, *J. Mater. Chem. A*, 2014, **2**, 3782-3794.

Figure captions

Fig. 1: Schematic representation of the complete synthesis of Pt/RG process.

Fig. 2: XRD pattern of graphite, GO, RGO, Pt/RG and Pt/RG-N.

Fig. 3: Raman spectra of graphite, GO, Pt/RG and Pt/RG-N.

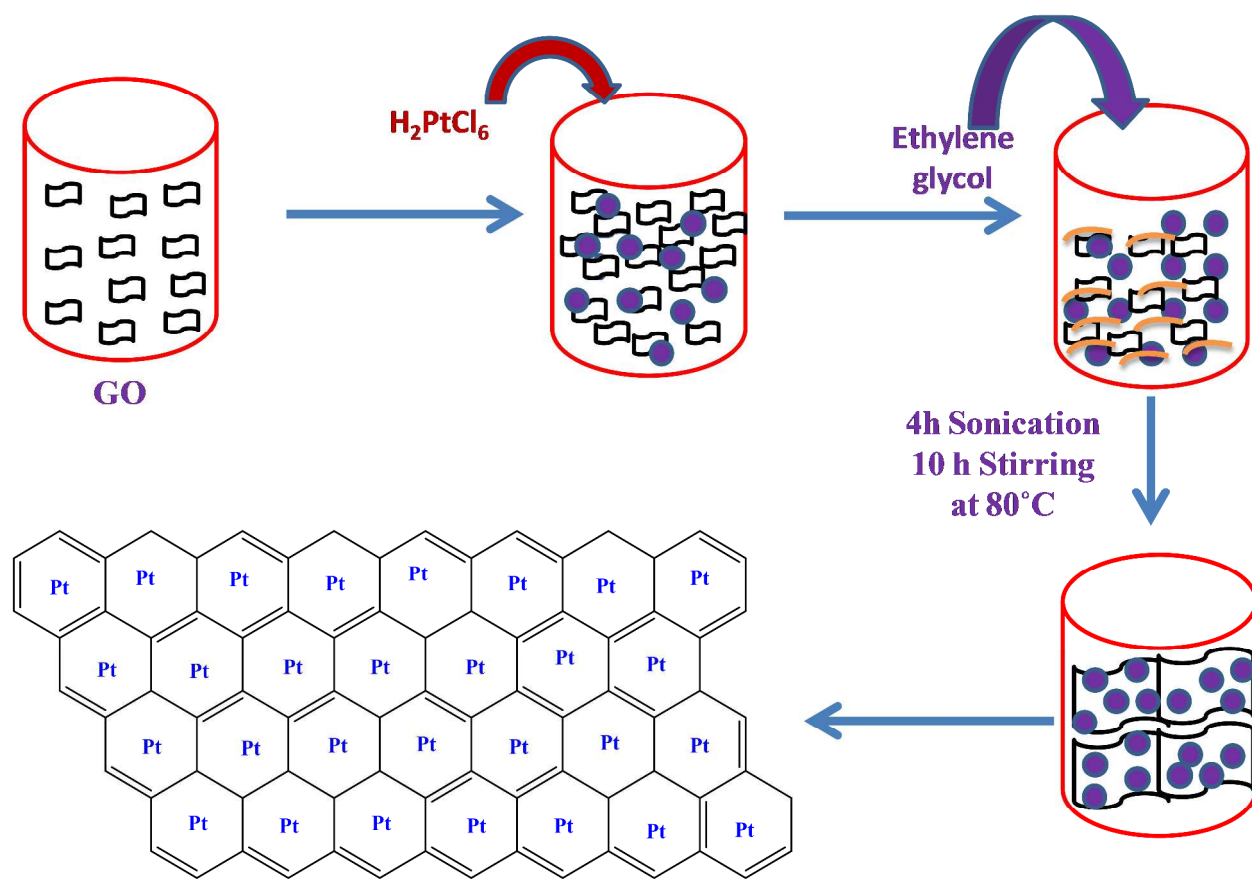
Fig. 4: FT-IR spectra of GO, Pt/RG and Pt/RG-N.

Fig. 5: FE-SEM image of (a) Pt/RG-N and (b) corresponding EDS confirms the presence of N and Pt in Pt/RG-N. TEM images of (c) Pt/RG and (d) Pt/RG-N and their corresponding SAED pattern and particle size distribution is shown as inset. HR-TEM image of (e) Pt/RG-N and fringes of Pt nano particles as shown in inset.

Fig. 6: XPS spectra of (a) Pt4f of Pt/RG and Pt/RG-N catalyst and a typical deconvoluted image shown as an inset (b) N1s spectra of Pt/RG-N catalyst.

Fig. 7: UV-Vis spectra for the successive reduction of 4- NA to p- PDA by NaBH₄ (25 mM) in the presence of Pt/RG of amount (a) 12.5 μg (b) 25 μg, (c) 37.5 μg and (a₁ to c₁) plot of ln Conc vs. time (min).

Fig. 8: Reaction mechanism involved in the reduction of 4-NA to p-PDA in the presence of NaBH₄ and Pt/RG catalyst. Results showed yellow colour 4-NA upon reduction changed to colorless p-PDA.

**Fig. 1**

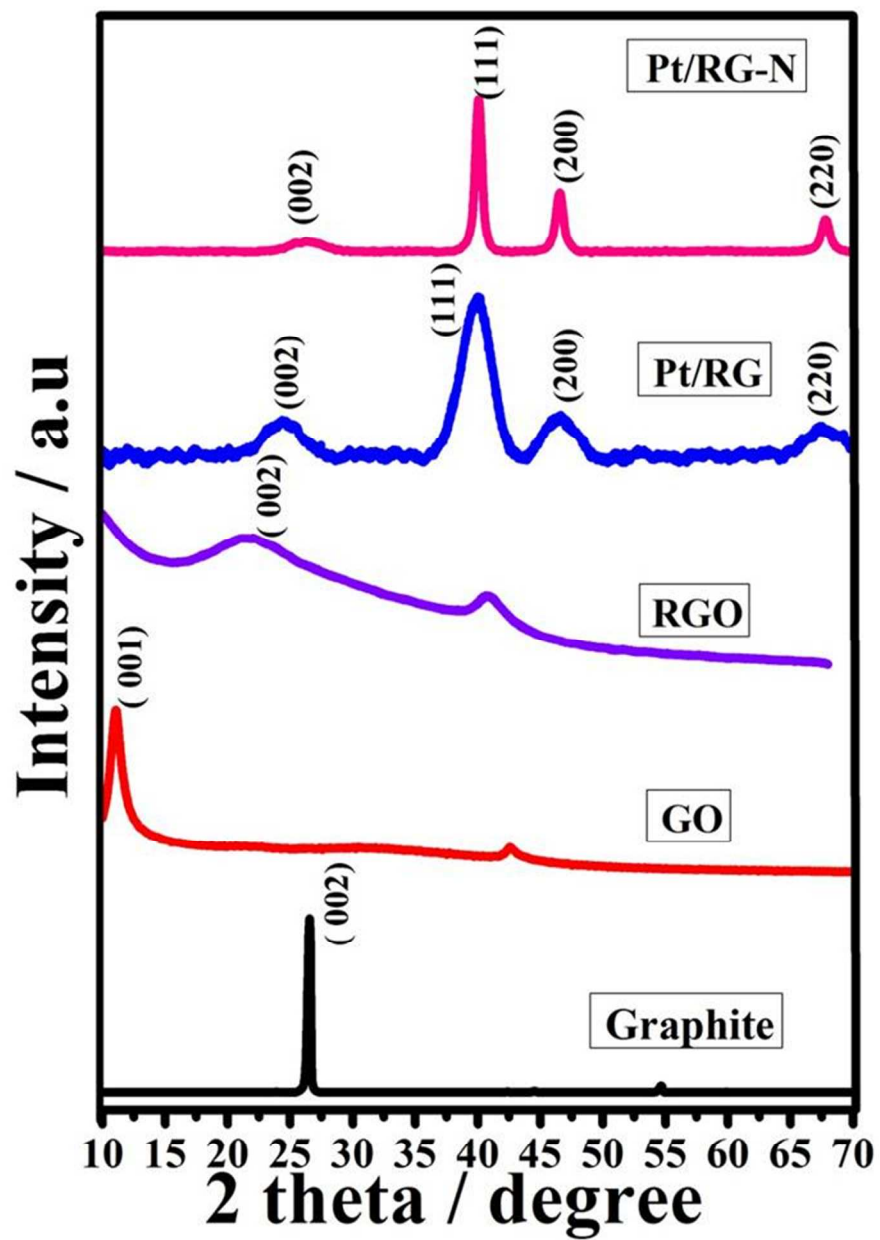


Fig. 2

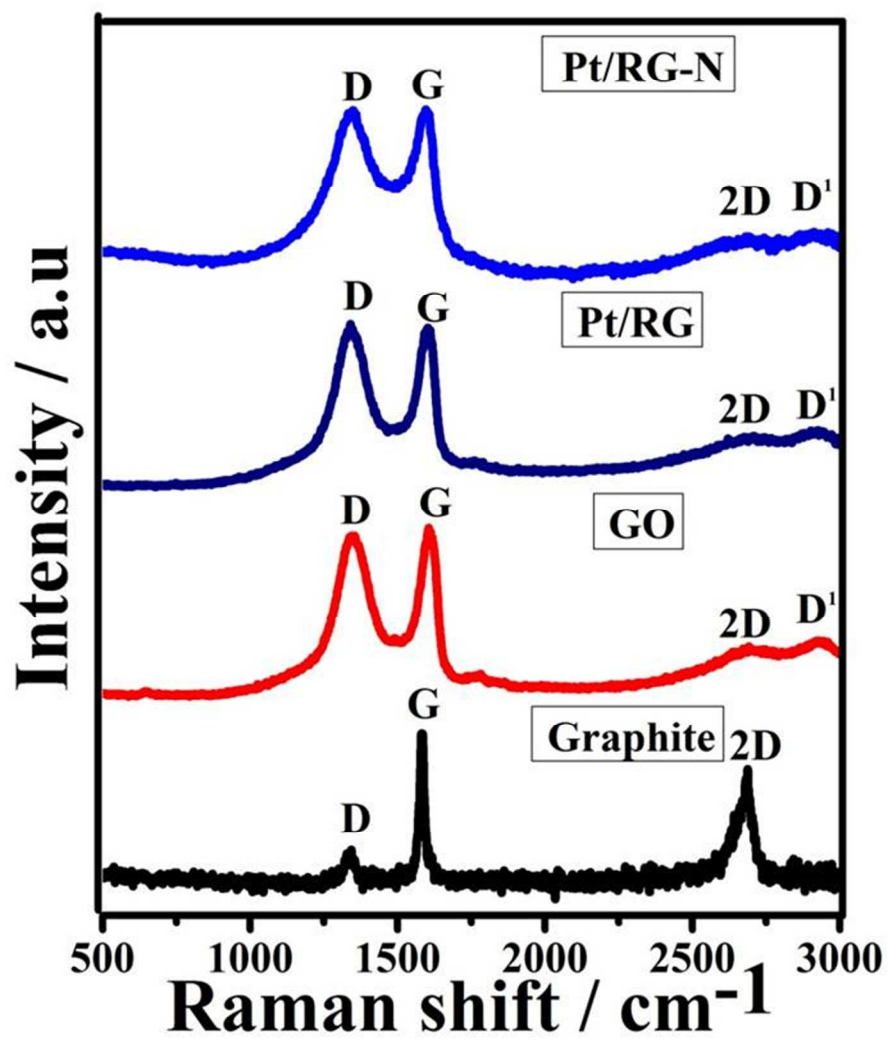


Fig. 3

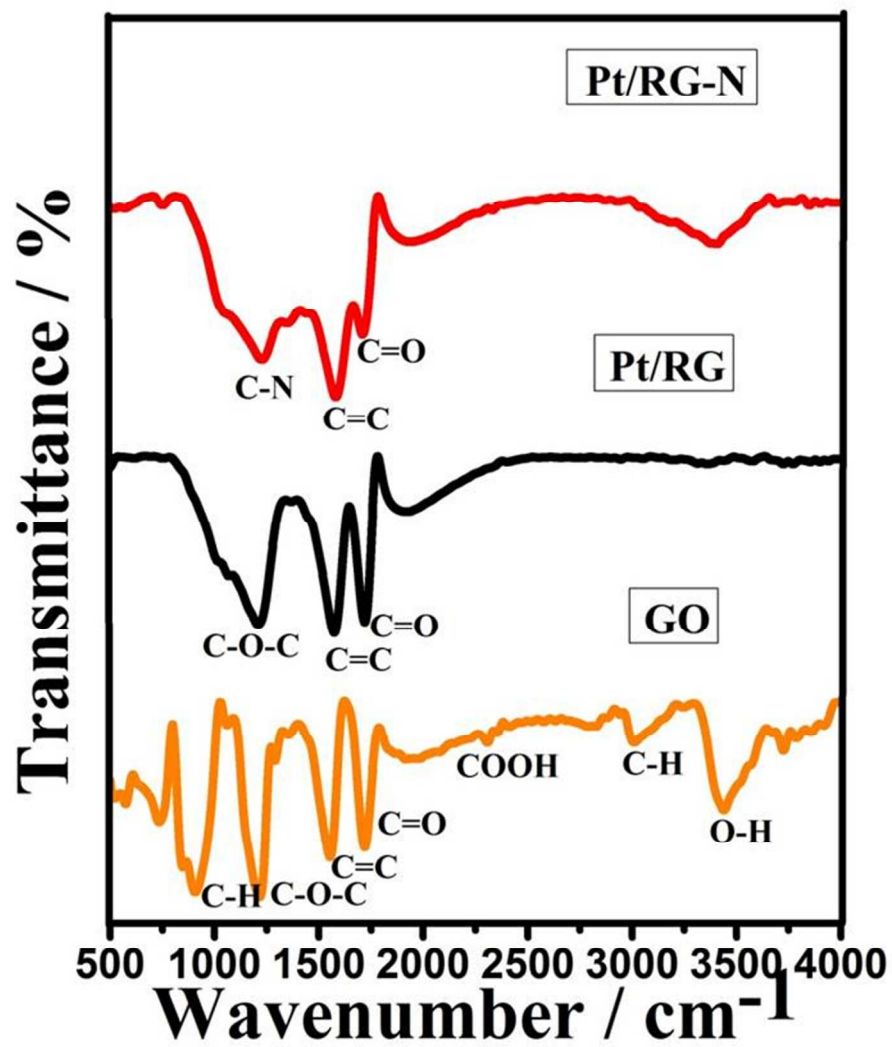


Fig. 4

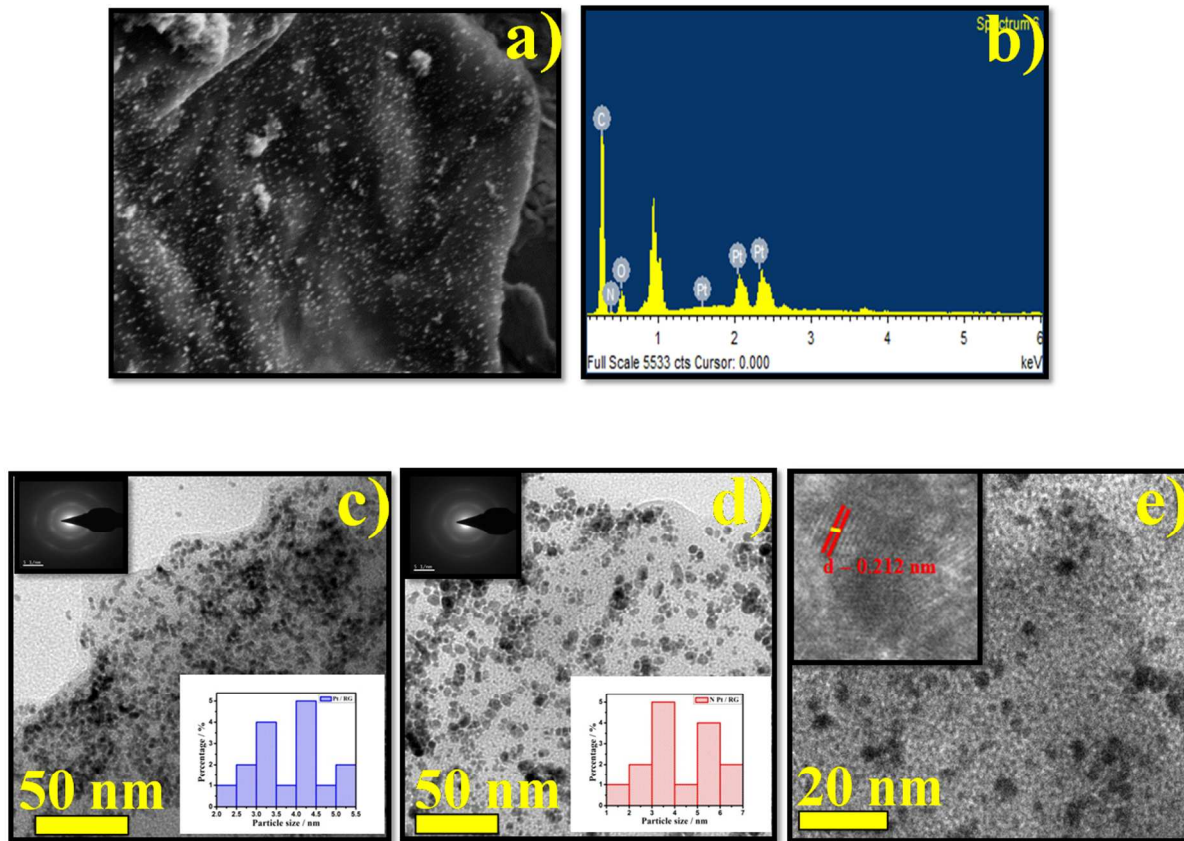


Fig. 5

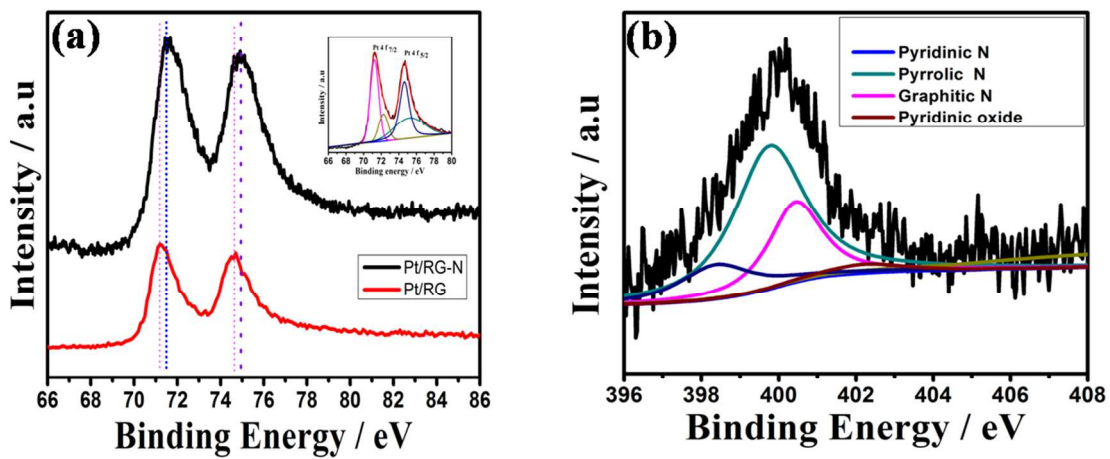


Fig. 6

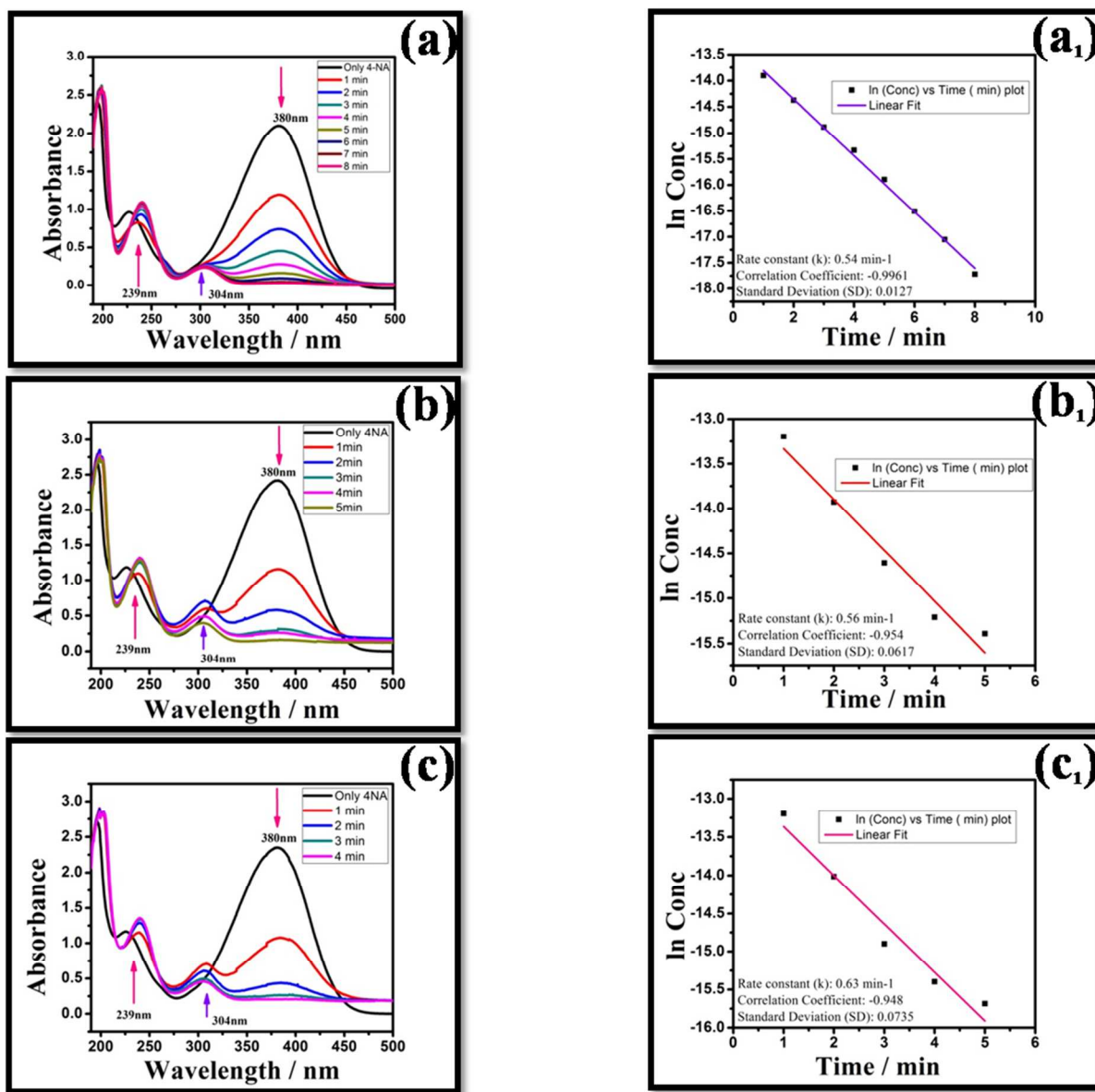


Fig. 7

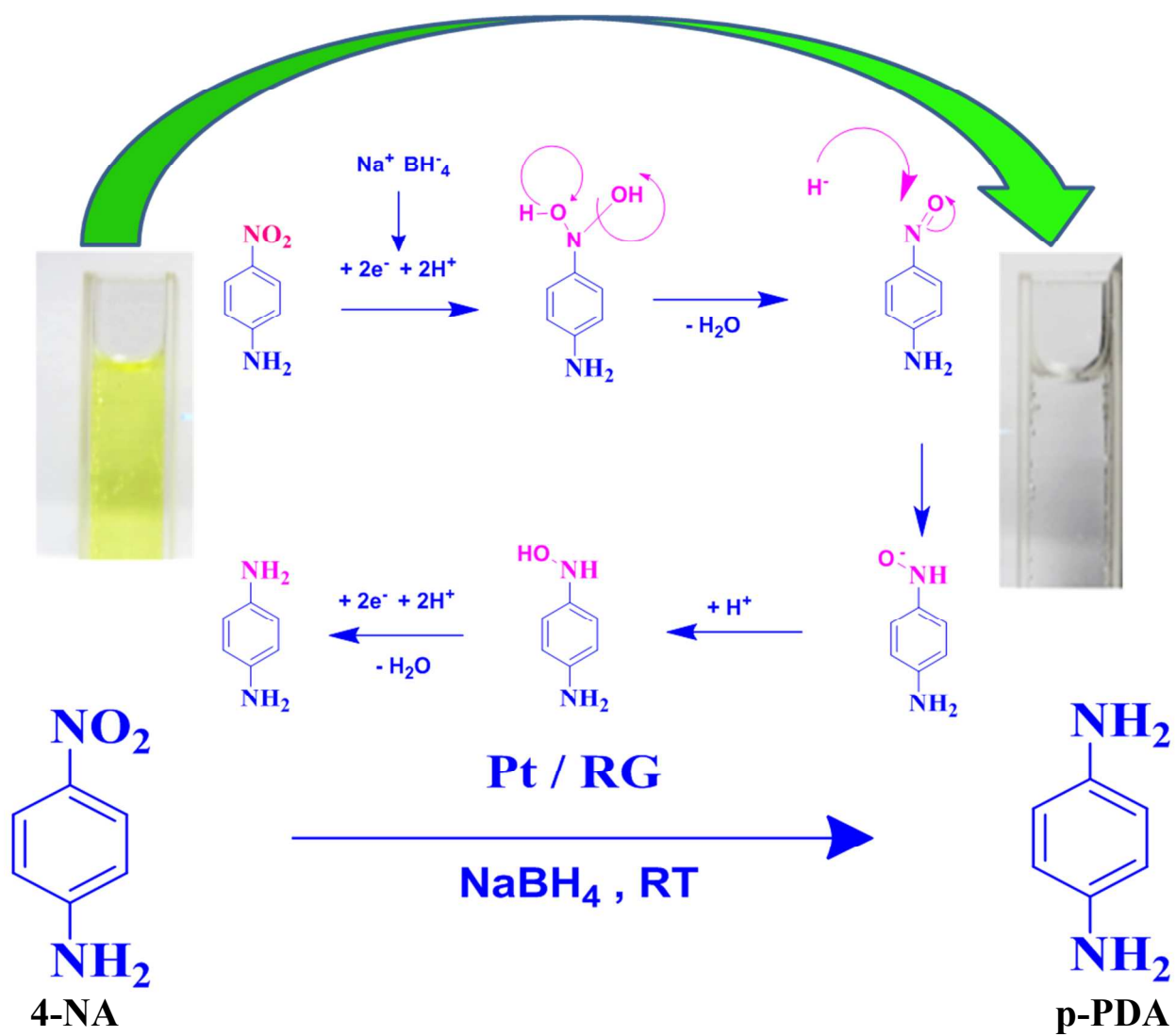


Fig. 8

Table 1: I_D / I_G ratio and crystallite size of GO, Pt/RG and Pt/RG-N as found from Raman spectra.

S.No	Sample	I_D/I_G	L_a (nm)
1.	GO	0.95	36.48
2.	Pt/RG	1.08	39.55
3.	Pt/RG-N	1.13	43.39

Table 2: Comparative study of pseudo first order rate constant of 4-NA reduction by Pt/RG catalyst in the present study and other reported nanocatalyst.

Catalyst	Initial concentration of 4-NA (mol/ L)	Concentration of NaBH₄	Amount of catalyst (µg / mL)	Rate constant (min⁻¹)	Reference
Pt / RG	1×10 ⁻³	10mM	12.5	25×10 ⁻²	This work
Pt / RG	1×10 ⁻³	20mM	12.5	29×10 ⁻²	This work
Pt / RG	1×10 ⁻³	25mM	12.5	54×10 ⁻²	This work
Pt / RG	1×10 ⁻³	25mM	25	56×10 ⁻²	This work
Pt / RG	1×10 ⁻³	25mM	25	63×10 ⁻²	This work
BSGN	1×10 ⁻³	-	-	24×10 ⁻²	[35]
Au - GO	1×10 ⁻³	-	-	9.4×10 ⁻²	[35]
Os NPs	1×10 ⁻³	-	-	3.87×10 ⁻²	[53]